Mechanism for Zr Poisoning of Al-Ti-B Based Grain Refiners

Y. Wang[1], C.M.Fang[1], L. Zhou[1], T. Hashimoto[2], X. Zhou[2], Q.M. Ramasse[3], Z. Fan[1]*
[1] BCAST, Brunel University London, Uxbridge, Middlesex UB8 3PH, UK
[2] School of Materials, University of Manchester, Manchester M13 9PL, UK
[3] SuperSTEM, STFC Daresbury Laboratories, Keckwick Lane, Warrington WA4 4AD, UK

*Corresponding author. Tel.: +44 1895 266406; Fax: +44 1895 269758; E-mail address: Zhongyun.Fan@brunel.ac.uk

Abstract

Al-Ti-B based master alloys have been widely used for grain refining of Al-alloys in industry for many decades. However, the effectiveness of such grain refiners is severely compromised when a few hundred ppm of Zr is present in the Al melt, and this phenomenon is referred to as Zr poisoning in the literature. So far the exact mechanisms for Zr poisoning are not clear albeit significant research effort on the subject in the last few decades. In this work we investigated the mechanism for Zr poisoning through extensive examinations of the Al/TiB_2 interface using the state-of-the-art electron microscopy and *ab initio* molecular dynamics simulations. We found that the presence of Zr in Al melts leads to (i) the dissolution of the Al_3Ti 2-dimensional compound (2DC) formed on the (0 0 0 1) TiB_2 surface during the grain refiner production process; and (ii) the formation of an atomic monolayer of Ti_2Zr 2DC on the (0 0 0 1) TiB_2 surface, which replaces the original Ti-terminated TiB_2 basal surface. This monolayer of Ti_2Zr not only has large lattice misfit (4.2%) with α-Al, but also is atomically rough, rendering the TiB_2 particles impotent for heterogeneous nucleation of α-Al. This work, in combination of our previous work, demonstrates that heterogeneous nucleation can be effectively manipulated, either enhanced or impeded, by chemical segregation of selected alloying/ impurity elements at the liquid/substrate interface.

Keywords: Heterogeneous nucleation; Grain refinement; Aluminium alloys; Zirconium poisoning.

1. Introduction

Grain refinement during casting of engineering alloys is usually desirable, since it results in not only a fine and equiaxed grain structure but also a significant reduction of casting defects, which in turn leads to an improved engineering performance [1]. As a common practice in the metal casting industry, grain refinement is usually achieved by chemical inoculation through addition of grain refiners. Among a series of Al-Ti-B based grain refiners developed for Al-alloys, Al-5Ti-1B (all compositions are in wt.% unless otherwise specified) master alloy has been the most widely used grain refiner, which contains potent TiB_2 particles for enhancing heterogeneous nucleation of α-Al grains [2]. Since the introduction of Al-Ti-B based grain refiners at the beginning of the 1950s [3], significant effort has been made to optimize their performance largely through a trial-and-error approach, and to understand the grain refining mechanisms, with both the theory and practice being extensively reviewed [2, 4-7]. However, only recently has the mechanism for grain refinement been made clear; i.e., formation of an atomic monolayer of Al_3Ti 2-dimensional compound (2DC) on the (0 0 0 1) TiB_2 surface is responsible for the high potency of TiB_2 particles for heterogeneous nucleation of α-Al [8].

Both alloying and impurity elements in Al-alloys are known to improve the grain refining

effectiveness of Al-Ti-B master alloys. However, the presence of solute elements is not always beneficial and the interaction between solute elements and TiB_2 particles sometimes renders TiB_2 particles impotent for heterogeneous nucleation. It has been reported that, in the presence of certain alloying or impurity elements in Al-alloys, such as Zr, Cr and Li, and high levels of Si, the effectiveness for grain refinement of Al-Ti-B master alloys can be dramatically reduced, resulting in a coarse and columnar grain structure in some cases [9-26]. This adverse effect on grain refinement is often referred to as "poisoning" in the literature.

Zr itself is usually considered to be a favorable solute element for grain refinement of Al-alloys since it has a relatively large growth restriction factor [27, 28], although its refining ability was found to be less than that of Ti [5, 25]. When the concentration of Zr is higher than the peritectic composition (0.11%), Al_3Zr forms as the primary phase, which acts as an effective substrate for heterogeneous nucleation of α-Al [29, 30]. It has also been shown that the grain refining effects of Zr and Ti are not additive and their combined effect is much less than either of the elements alone [5, 25].

However, Zr-containing Al-alloys are usually difficult to grain refine using the Al-Ti-B grain refiners. Jones and Pearson [9] observed that it was not possible for the grain size of an Al-5Zn-1.5Mg-0.2Zr alloy to be refined below 250 μm by Al-5Ti-1B inoculation. By increasing the level of Al-5Ti-1B addition, the grain size was reduced to below 250 μm only when the holding time was shorter than 10 minutes, and a considerably larger grain size was observed in samples with prolonged holding time [9]. Birch and Fishers [10] reported the poisoning effect in Zr-containing commercial 7xxx Al-alloys inoculated with Al-5Ti-1B grain refiner, and similar observations were reported by Ahmadey *et al.* [11] and Kearns and Cooper [12] in 7050 Al-alloy containing 0.10-0.13% Zr. Results of Birch and Cowell [13] and Abdel-Hamid [14, 15] also confirmed the poisoning effect of Zr in Al-alloys. Furthermore, it has been reported that the poisoning effect of Zr was promoted by the presence of Li as an alloying element in Al-alloys [16].

Impurities were found to affect Zr poisoning. Spittle and Sadli [17] investigated the effect of Fe, Si, Cr, and Zr on the grain refinement of high purity Al (HP-Al) inoculated with Al-5Ti-1B grain refiner. They concluded that Zr addition results in a poisoning effect with the presence of Fe and Si. However, Zr alone in HP-Al was found to be beneficial to grain refinement by the Al-5Ti-1B grain refiner. In another report, Spittle and Sadli [18] also studied the influence of various alloying elements, including 0.05% Zr, on the grain refinement of HP-Al, and found that the grain size of binary Al-alloys is strongly dependent on the magnitude of the constitutional undercooling parameter. Qiu *et al.* [19] proposed a co-poisoning mechanism by Zr and Ti when a certain amount of Fe impurity was present in terms of crystallographic analysis. Johnsson [20] found that, for hypoperitectic Al-alloys, Zr and Ti in the liquid cooperated to promote grain refinement, while in hyperperitectic Al-alloys grain refinement deteriorated due to the formation of a mixed aluminide phase, $(Ti_{1-x}Zr_x)Al_3$. It was speculated that the formation of the ternary aluminide removes Ti dissolved in the melt, resulting in reduced growth restriction during the growth of α-Al dendrites.

A few hypotheses have been proposed to explain the poisoning effect of some solute elements on the grain refining effectiveness of Al-Ti-B master alloys. In their work on the effect of various alloying elements on grain refinement, Jones and Pearson [9] attributed the poisoning effect of Zr to the formation of ZrB_2 coatings on the TiB_2 surface, because ZrB_2 is thermodynamically more stable than TiB_2. They believed that ZrB_2 coatings prevent TiB_2 from acting as a nucleating site for the α-Al due to its larger lattice parameters than TiB_2, although no evidence of the formation of ZrB_2 was presented. Trying to explain the poisoning effect of Zr and Cr, Abdel-Hamid [14] proposed that some of the Ti atoms in Al_3Ti and TiB_2 crystals were replaced by poisoning elements, such as Zr, Cr, etc., resulting in the formation of a less potent Al-Ti-Zr ternary compound. Murty and his co-workers [5, 21, 22] shared this point of view in their explanation of the poisoning effect of Cr and

Zr. The mechanism involving the formation of ternary aluminides was also supported by Johnsson [20] who suggested that the poisoning effect of Zr was associated with the reduced potency of Al_3Ti through the formation of $(Ti_{1-x}Zr_x)Al_3$. Bunn *et al*. [31] observed the presence of Zr in Al_3Ti and attributed the poisoning effect to the modification of both Al_3Ti and TiB_2 by Zr. In addition, the formation of $(Ti_{1-x}Zr_x)Al_3$ would reduce the Ti concentration in the melt and thus the growth restriction, which is also believed to be an important factor for grain refinement. However, Bunn *et al*. [31] realized that reduction in growth restriction arising from reduced solute concentrations in the melt was not the dominant factor in Zr poisoning and that the poisoning was mainly attributed to the interaction between Zr and the nucleating substrates. Another explanation for the poisoning effect of Zr and Cr was proposed by Jones in his hyper-nucleation theory [32], which involves the atomic size mismatch between Zr or Cr and the solvent Al.

Although the exact mechanism for the poisoning effect is so far unclear, it is generally accepted that poisoning is mainly due to the interaction of these alloying elements, Zr, Cr, Si and Li, with the nucleating particles, such as Al_3Ti and TiB_2 [9, 14, 31, 33]. It is anticipated that such interaction may give rise to the formation of complex aluminides, borides and silicides, which have a poor potency for nucleating α-Al grains, on the surface of nucleating particles.

The loss of nucleation potency through poisoning is known to be time dependent; i.e., grain size increases with holding time after addition of grain refiner. Experimental work [9, 31] showed that the poisoning effect increases with holding time after the addition of Zr, being consistent with progressive substitution of Ti atoms with Zr atoms. In general, loss of nucleation potency by poisoning is non-recoverable, unlike gravity-induced fading (i.e., settling of nucleant particles), which can be recovered by stirring the melt prior to casting.

Zr is an important trace alloying element in some 2xxx and 7xxx series Al-alloys due to its contribution to dispersion strengthening and impedance of dynamic recrystallization. For example, typical 7xxx series alloys contain about 0.12% Zr for dispersion strengthening. Problems can be encountered during direct chill (DC) casting of such alloys, where the performance of Al-Ti-B grain refiner is significantly reduced due to the Zr poisoning effect. Considerable work has been carried out to reduce or eliminate such poisoning. Increasing the addition level of Al-5Ti-1B master alloy has been shown to be a way to improve the grain refining response [9, 33], although the accumulation of non-active TiB_2 particles in the alloy causes serious concern. Another approach to overcome the problem is to use alternative grain refiners, such as Al-Ti-C based master alloys [34-38]. As a promising grain refiner, Al-Ti-C master alloy has been reported to be resistant to Zr poisoning to a certain extent, although there are some controversies between different investigators [38]. In a 7xxx Al-alloy containing 0.06% Zr, addition of Al-3Ti-0.15C master alloy has been shown to result in a very fine grain structure without twin columnar growth [34]. Schneider *et al*. [35] also found that the grain refining effect of Al-5Ti-0.25C grain refiner was better than that of Al-5Ti-0.2B in a Zr-containing 7050 alloy at the same addition level. However, experimental study [37] has demonstrated that Al-Ti-C master alloy may be poisoned in the presence of Zr. The grain refining ability of Al-5Ti-0.4C master alloy (0.2% addition) was reported to diminish when 0.12% Zr was added to the melt [38]. It was suggested that Zr interacted with both $TiAl_3$ and TiC phases.

In the present work, extensive electron microscopy has been carried out focusing on the Al/TiB_2 interface, in order to reveal any possible modification caused by interaction between Zr and TiB_2 at the interface. An *ab initio* molecule dynamics method is employed to simulate the structure and stability of the segregation layer at the interface at temperature above the liquidus of Al in accordance with the experimental observation. Mechanism underlying Zr poisoning is discussed in the context of Zr segregation at the Al(liquid)/TiB_2 interface and its consequence on the potency of TiB_2 particles for heterogeneous nucleation of α-Al.

2. Experimental

2.1 Materials

Commercial purity aluminium (CP-Al, > 99.86% Al) and Al-10Zr master alloy were used for all the experiments in this work. TiB_2 particles were introduced to the CP-Al melt through the addition of 0.1% of commercial Al-5Ti-1B grain refiner rods supplied by LSM (Rotherham, UK). In order to assess the effect of Zr on the effectiveness of the grain refiner, Zr was added to the CP-Al melt at concentrations between 0.058% and 0.450%. The chemical compositions and impurities of the materials used in this work are given in Table 1.

2.2 Grain size assessment

The standard TP-1 test [39] was used to assess the grain size by providing a consistent cooling rate of 3.5 K/s at the central region of the cross-section 38 mm from the bottom of the TP-1 cast sample. Al-Zr melts with varying Zr concentrations were held isothermally at 800°C for 4 hours followed by the addition of 0.1% Al-5Ti-1B grain refiner. After holding for 1 more hour, the Al-Zr alloy melt inoculated with Al-5Ti-1B master alloy was cast into the pre-heated TP-1 mould (350°C) which was immediately cooled by water spray with a controlled water flow rate of 3.8 l/min. Such TP-1 tests were also carried out on CP-Al with no addition of Zr for comparison.

Quantitative metallography for grain size assessment was performed by examining the grain structure of the transverse section 38 mm from the base, and the longitudinal section of the lower part of the TP-1 sample. The specimens for the grain size assessment were prepared using standard metallographic techniques. Electro-polishing was performed prior to anodizing with Barker's reagent (5 ml HBF_4 + 200 ml distilled water) to show the grains with different orientations. A Zeiss optical microscope fitted with the Axio Vision 4.3 image analysis system was used for the grain size assessment under polarized light. A mean linear intercept technique was used to quantify the grain size with measurement of at least 500 grains.

2.3 High resolution TEM/STEM

A pressurised melt filtration technique was used to collect the TiB_2 particles introduced to the alloy melt through the addition of the commercial Al-5Ti-1B grain refiner, in order to facilitate direct examinations using advanced electron microscopy. In this process, Al-Zr alloy melt inoculated with 0.2% Al-5Ti-1B grain refiner was transferred into the crucible in the pressure chamber. Argon was introduced to force the melt to flow through a porous filter attached to the bottom of the crucible. TiB_2 particles were thus collected above the filter together with the residual melt. The solidified material immediately above the filter, which contained the locally concentrated TiB_2 particles, was subjected to examination. A detailed description of the melt filtration technique can be found elsewhere [40, 41].

Thin foil specimens for transmission electron microscopy (TEM) and scanning transmission electron microscopy (STEM) were prepared from 3 mm diameter discs sliced from the filtered residue material. The discs were ground to a thickness less than 60 μm before further thinning by Ar ion beam milling using a Gatan precision ion polishing system (PIPS) under a voltage of 1.0-5.0 kV and an incident beam angle of 3-5°. Traditional high resolution TEM analysis was conducted on a JEOL 2100F microscope operated with an accelerating voltage of 200 kV. Atomic resolution STEM with Z-contrast high-angle annular dark filed (HAADF) imaging was carried out on an aberration (Cs)-corrected FEI Titan 80-200 instrument equipped with Super-X energy dispersive x-ray spectroscopy (Super-X EDS) system, operated with an accelerating voltage of 200 kV. Further STEM of a higher resolution was conducted using Nion Ultra-STEM 100 instrument (2nd

generation) at the SuperSTEM Centre (Daresbury, UK). This microscope was equipped with a field emission gun operated at 100 kV, and a Nion spherical aberration (Cs) corrector and electron energy loss spectroscopy (EELS) system. Super-X EDS mapping and atomic resolution EELS mapping were conducted to obtain compositional profiles across Al/TiB_2 interface.

Simulation of STEM-HAADF images was conducted using the QSTEM multislice simulation package developed by Koch [42], and the simulated results were compared to the STEM HAADF images obtained experimentally using Cs-corrected high resolution STEM.

2.4 *Ab initio* molecular dynamics simulations

Ab initio molecular dynamics (MD) simulations were carried out using the code VASP (Vienna *ab initio* Simulation Package) [43, 44], which employs the *ab initio* density functional theory (DFT) within the projector-augmented wave (PAW) framework [45, 46]. The exchange and correlation terms were described using the generalized gradient approximation (GGA-PBE) [47]. A cut off energy of 320 eV and only Γ-point in the BZ [48] were used. The liquid Al was generated by equilibrating for about 10 picoseconds (ps) at 3000 K, followed by cooling down to and equilibrated at a designated temperature for 10ps. The liquid Al obtained in this way was brought in contact with the TiB_2 substrate and then equilibrated at the same temperature for 10ps to ensure equilibrium. The time-averaged method was employed to take samples with over several ps (2000 to 3000 steps, 1.5fs/step) to satisfy the statistics. The substrate and liquid atoms were fully relaxed during the simulations.

3. Results

3.1 Confirmation of Zr poisoning

Prior to investigation of the poisoning mechanism, it is important to confirm the Zr poisoning effect through designed solidification experiments. Figs. 1a and 1d show the macrostructure of CP-Al solidified under TP-1 conditions. Both the transverse and longitudinal sections show a coarse columnar grain structure. Addition of 0.1% commercial Al-5Ti-1B grain refiner to the CP-Al melt resulted in a fine and fully equiaxed grain structure (Figs. 1b and 1e), with the average grain size being 175±25 μm. This suggests that the commercial Al-5Ti-1B grain refiner used in this experiment is effective for grain refinement of CP-Al. However, the macrostructure of Al-0.058Zr alloy inoculated with 0.1% Al-5Ti-1B grain refiner has a coarse columnar grain structure (Figs. 1c and 1f). This indicates that the effectiveness of the grain refiner was reduced dramatically due to the presence of 580 ppm Zr in the melt, confirming the poisoning effect of Zr. With further increase of Zr concentration up to 0.45%, the macrostructures of Al-Zr alloys inoculated with 0.1% Al-5Ti-1B grain refiner remain coarse and columnar, and the width of the columnar grains increases with increasing Zr concentration (Fig. 2). This suggests that the effect of Zr poisoning increases with increasing Zr concentration.

3.2 Segregation of Zr atoms on TiB_2 surface in dilute Al-Zr alloys

The reference point for our investigation is the TiB_2 particles brought into the Al melt by the commercial Al-5Ti-1B grain refiner. It was confirmed in our previous work [8] that the TiB_2 particles in such grain refiner are extremely potent for heterogeneous nucleation of α-Al due to the presence of Al_3Ti 2DC on the (0 0 0 1) TiB_2 surface. High temperature, high concentration of Ti and prolonged reaction time in the fabrication processing of the grain refiner ensures the formation of the Al_3Ti 2DC. A well-defined orientation relationship (OR): (0 0 0 1)[1 1 -2 0] TiB_2 // (1 1 1) [0 -1 1] Al was observed readily in the CP-Al sample inoculated by the Al-5Ti-1B grain refiner.

In order to examine any possible modification of the TiB_2 surface due to the presence of Zr in the alloy melt, TiB_2 particles in the Al-Zr alloy were collected and examined in detail by SEM and TEM/STEM, focusing on their faceted surfaces. It was confirmed that the terminating facets of the TiB_2 particles are {0 0 0 1} basal and {1 0 -1 0} prismatic planes. Their average size is 0.2~3.2 μm in diameter, which is the typical size range observed in a commercial Al-5Ti-1B grain refiner [49]. No obvious change in size and morphology was observed before and after the Zr addition by SEM examination. However, TEM/STEM examination has revealed several interesting facts: (i) the well-defined OR between TiB_2 and Al was not observed in the Al-Zr alloy inoculated by Al-5Ti-1B refiner, although as many as 100 TiB_2 particles in total were examined in multiple thin foil TEM specimens; (ii) the original Al_3Ti 2DC was not observed on (0 0 0 1) TiB_2 surface; and (3) the original Ti-terminated (0 0 0 1) TiB_2 surface is replaced by a new segregation layer.

Atomic scale examination of this new segregation layer (STEM HAADF images in Fig. 3) reveals that it is an atomic monolayer of chemical segregation on the (0 0 0 1) TiB_2 surface, as evidenced by the atomic columns having a brighter contrast than that of the Ti columns in TiB_2 when the TiB_2 is viewed along both [1 1 -2 0] (Fig. 3a) and [1 0 -1 0] (Fig. 3c) directions. The α-Al is oriented away from any low index zone direction in both Figs. 3a and 3c, suggesting that this particular TiB_2 particle did not participate in grain initiation during solidification. The higher brightness of atom columns in the segregation layer indicates that heavier (than Ti) atoms exist in these columns (large green spheres represent heavier atom X in Figs. 3b and 3e). Particularly, on tilting the specimen by 30° from [1 1 -2 0] to [1 0 -1 0] TiB_2, the brightness of the segregation layer is no longer uniform as shown more clearly by the SuperSTEM HAADF image in Fig. 3d. Instead, it has a periodic variation with two darker atomic columns between the two brighter atomic columns as illustrated schematically in Fig. 3e. The periodic variation in brightness in the HAADF image indicates that there are at least two types of atoms in the segregation layer, with their arrangement being ordered in 2D. In addition, experimental measurement shows that the spacing between the segregation layer and its closest Ti layer in TiB_2 was slightly larger than the spacing between two Ti layers in TiB_2, i.e., 0.34±0.01 nm compared with 0.32 nm. These results suggest that the surface segregation layer is an ordered 2DC, in which the atoms are arranged in a hexagonal configuration, following that of Ti atoms in the (0 0 0 1) TiB_2 terminating plane.

High resolution Super-X EDS analysis using aberration (Cs)-corrected STEM instrument was performed to identify the chemical nature of the segregation layer on the TiB_2 surface. An example of such analysis is given in Fig. 4. The elemental mapping across the Al/TiB_2 interface shows the segregation of Zr atoms (Fig. 4b) at the interface, corresponding to the brighter contrast of the segregation layer in the HAADF image (Fig. 4a). No Zr segregation was observed on {1 0 -1 0} prismatic planes of the TiB_2 particles in this work, suggesting that segregation of Zr atoms is selective, depending on atomic configuration of the terminating surfaces of TiB_2. In addition, the presence of Al and Ti atoms in the segregation layer cannot be conclusive due to the existence of Al in the Al matrix and Ti in the TiB_2 substrate (Figs. 4c and 4d). Furthermore, particular attention was paid to the potential segregation of the main impurity elements in the alloy, such as Fe and Si. The EDS mapping results in Figs. 4e and 4f do not suggest any existence of either Fe or Si in the segregation layer.

Intuitively, one would not expect that the basal surface of all the TiB_2 particles to be entirely covered by the Zr-containing segregation layer. Indeed, it was occasionally found that some of TiB_2 particles were covered only partially by the segregation layer on their (0 0 0 1) surface. For instance, Fig. 5 shows that Zr segregation occurs on the left hand side of the (0 0 0 1) TiB_2 surface, confirmed by the specific periodic pattern of brightness in the HAADF image in Fig. 5a and the corresponding Zr elemental map from Super-X EDS analysis in Fig. 5b. Again Figs. 5c and 5d show no existence of Fe or Si in the segregation layer.

3.3 Chemistry and structure of Zr segregation layer

From the above experimental findings by the direct STEM observation and EDS analysis (Figs. 3-5), the segregation layer has the following unique characteristics: (i) it is an atomic monolayer; (ii) it is a 2-dimensional compound (2DC) in which the atoms have a hexagonal arrangement; and (iii) it contains Zr and one or more other elements. Based on the compositions of CP-Al and the master alloys used in this work (Table 1), other possible elements in the segregation layer may include Ti, Al, Fe and Si. However, Fe and Si are ruled out by the EDS results (Figs. 4 and 5). The possibility of Al can also be eliminated by the fact that Al atoms do not substitute Ti atoms in the Ti-terminated (0 0 0 1) TiB_2 surface as presented in our previous work [8], and this is consistent with the thermodynamic analysis that TiB_2 is more stable than AlB_2 (ZrB_2 is thermodynamically more stable than TiB_2 [9]). Therefore, the only possibility left is that the segregation layer contains 2 elements: Zr and Ti, with the atomic ratio of Zr/Ti being 1:2 according to the brightness pattern in the HAADF images (Figs.3a, 3c and 3d). Based on the above analysis, it can be concluded that the segregation layer is Ti_2Zr 2DC.

The atomic arrangement in the Ti_2Zr 2DC can therefore be constructed, as shown in Fig. 6. Figs. 6a and 6b show the atomic arrangement of (0 0 0 1) TiB_2 plane and Ti_2Zr 2DC, respectively, whilst Figs. 6c and 6d show the side view of the Ti_2Zr 2DC on the top of TiB_2 viewed along [1 1 -2 0]TiB_2 and [1 0 -1 0]TiB_2 directions, respectively. It is seen in Fig. 6b that, in the Ti_2Zr 2DC, every atomic column along direction A has the same Ti:Zr ratio (2:1), whilst there are two Ti atomic columns between the Zr ones along direction B (directions A and B are paralleled to [1 1 -2 0]TiB_2 and [1 0 -1 0]TiB_2 directions, respectively). Such atomic configuration produces the uniform and periodic Z-contrast brightness pattern as shown in Figs. 6c and 6d, which are consistent with those observed experimentally along these two directions (Figs. 3a, 3c and 3d). Fig. 6e presents a 3D construction of the Ti_2Zr 2DC on the (0 0 0 1) TiB_2 surface. The full coherency between Ti_2Zr 2DC and the Ti-terminated (0 0 0 1) TiB_2 surface suggest that the "lattice parameters", i.e., the inter-atomic spacing, for the Ti_2Zr 2DC equals to the a-value (a = 0.3030 nm) of the lattice constants of TiB_2.

Using the QSTEM multi-slice simulation package developed by Koch [42], simulation of STEM HAADF images was performed in order to validate the established characteristics of the segregation layer. A hybrid lattice structure composing of the Ti_2Zr 2DC on the (0 0 0 1) TiB_2 surface was established according to the analysis above, as shown schematically in Fig. 6. The parameters used for the simulation were Cs = -0.1 mm, Cc = 1.4 mm, Defu-schezer convergent angle = 20 mrad, specimen thickness = 50 nm. Fig. 7 compares the simulated STEM HAADF images with the experimental ones, along both [1 1 -2 0] and [1 0 -1 0] directions of TiB_2. The good agreement between the simulated images and the STEM HAADF images in Fig. 7 confirmed that the segregation layer is Ti_2Zr 2DC with an atomic configuration as shown in Fig. 6b.

3.4 The nature of Ti_2Zr 2DC

To understand the influence of TiB_2 substrate with Ti_2Zr 2DC on heterogeneous nucleation of α-Al, knowledge of the atomic ordering in the liquid Al adjacent to the TiB_2 substrate at a temperature close to the alloy liquidus is important. Therefore, *ab initio* MD simulations were performed for the Al(liquid)/TiB_2 (Ti_2Zr 2DC) system at 900 K, 1000 K and 1200 K, respectively. A snapshot of the system equilibrated at 1000 K viewed along the [1 0 -1 0] TiB_2 direction is shown in Fig. 8a. Fig. 8b shows the atomic density profiles of the liquid Al adjacent to the Al(liquid)/TiB_2 (Ti_2Zr 2DC) interface equilibrated at the three different temperatures. It is seen from Fig. 8a that the Zr atoms in the Ti_2Zr 2DC are protruded into the liquid Al. This protrusion of Zr atoms is quantified by the atomic density profile (Fig. 8b) where the atomic density peak for Ti_2Zr 2DC is separated into two sub-peaks marked as Ti and Zr. The central positions of the Zr atoms are 0.45 Å away from that of the Ti atoms, which represents 19% of Al (1 1 1) d-spacing (0.2338 nm). Therefore, it can be

concluded that the Ti_2Zr 2DC formed on the (0 0 0 1) TiB_2 surface has a 19% surface roughness at atomic level. Consequently, the atomic ordering in the liquid Al adjacent to the liquid/substrate interface is significantly weakened; only two clear peaks are shown in the atomic density profile (Fig. 8b) compared with 6 peaks with an atomically flat substrate surface [50]. Furthermore, Fig. 8b suggests that the atomically rough Ti_2Zr 2DC is highly stable over a broad range of temperatures, 900~1200 K.

4. Discussion

4.1 Zr segregation on TiB_2 surface

Our previous work [8] revealed that a Ti segregation layer on the (0 0 0 1) TiB_2 surface in Zr-free CP-Al melts inoculated by Al-5Ti-1B grain refiner is an Al_3Ti 2DC. Compared with the Ti segregation layer, the Zr segregation layer observed in this work is substantially different. The Al_3Ti 2DC is situated on top of the Ti-terminated (0 0 0 1) TiB_2 surface with a smaller plane spacing of 0.25±0.01 nm. In contrast, the Ti_2Zr 2DC forms a new terminating surface of the TiB_2 particle with an enlarged atomic plane spacing of 0.34 nm compared with the Ti-layer spacing (0.32 nm) in the TiB_2 structure. This larger spacing (by 0.2 Å) observed experimentally at room temperature is in qualitative agreement with the results (by 0.45 Å) obtained by *ab initio* MD simulations at 1000 K (Fig. 8). This larger spacing can be attributed to the larger atomic size of Zr than that of Ti and stronger chemical attraction between Zr and Al atoms compared with that between Ti and Al atoms.

Crystal structures of various binary and ternary Ti-Zr intermetallic compounds have been investigated previously, with ω-Ti_2Zr intermetallic phase being particularly relevant to this work [51-54]. The experimental investigations [51-53] and first-principles DFT study [54] have confirmed that, as a metastable phase, ω-Ti_2Zr phase has a hexagonal structure (AlB_2 type) with the lattice parameters: a=0.4795 nm and c=0.3020 nm [51], which may vary slightly in different work. As shown in Fig. 9a, the unit cell of the ω-Ti_2Zr phase contains one Zr atom at {0, 0, 0} position forming the (0 0 0 1) Zr plane and two Ti atoms at {1/3, 2/3, 1/2} and {2/3, 1/3, 1/2} positions forming the (0 0 0 1) Ti plane. Figs. 9b and 9c show the arrangement of Zr atoms and Ti atoms in the (0 0 0 1) Zr and (0 0 0 1) Ti planes of ω-Ti_2Zr phase, respectively. In fact, the structure of the Ti_2Zr 2DC on the TiB_2 surface based on our HRTEM observations (Fig. 6b) can be constructed by superimposition of a (0 0 0 1) Ti plane and its neighbouring (0 0 0 1) Zr plane to form a 2D superstructure, as schematically shown in Fig. 9d. The superimposition of the two atomic layers is feasible because neither Zr nor Ti atoms in ω-Ti_2Zr phase are closely packed in their respective crystal planes. It should be pointed out that the Ti_2Zr 2DC does not necessarily need to be an actual plane of the 3D (bulk) ω-Ti_2Zr phase. The "lattice parameter" of the Ti_2Zr 2DC structure constructed according to the ω-Ti_2Zr phase is a = 0.277 nm at room temperature [51], which is smaller than the a-value 0.3020 nm of TiB_2 lattice parameters. However, this discrepancy may become smaller when thermal expansion of both Ti_2Zr 2DC and TiB_2 and structural relaxation of the Ti_2Zr 2DC at the interface at the nucleation temperature are taken into full consideration. More importantly, the experimentally observed "lattice parameter" for the Ti_2Zr 2DC in this work equals to the a-value 0.3020 nm of the lattice parameters of TiB_2, because the 2DC is totally coherent with the (0 0 0 1) Ti plane of TiB_2.

Formation of the 2DC through chemical segregation in a dilute Al-Zr solution is expected to be time dependent, giving rise to the partial formation of the Ti_2Zr 2DC on the TiB_2 surface (Fig. 5). Further penetration of Zr atoms into the TiB_2 crystal structure beyond the (0 0 0 1) Ti-terminated surface is difficult due to the presence of the layer of B atoms beneath the Ti_2Zr 2DC, which have strong covalent bonds between the B atoms and the Ti atoms below them. This means that the formation of both bulk (3D) ZrB_2 and $(Zr_xTi_{1-x})B_2$ are kinetically unfavourable even if they are thermodynamically feasible as suggested in the literature [9, 55, 56].

4.2 Effect of impurities (Fe and Si) on poisoning

Spittle and Sadli [17] suggested the possible involvement of Fe and Si in delivering the poisoning effect of Zr. However, the main impurities Fe and Si in the CP-Al used in this study does not show any evidence of their segregation on the (0 0 0 1) TiB_2 surface (Figs.4 and 5). In fact, Fe segregation was observed on {1 0 -1 0} prismatic planes of TiB_2, although Si segregation was not observed on either basal or prismatic surfaces of TiB_2 particles. Fig. 10 is an example of STEM/EDS analysis across the Al/(1 0 -1 0)TiB_2 interface, showing Fe segregation, but no segregation of Zr and Si. As the heterogeneous nucleation of α-Al takes place only on {0 0 0 1} basal plane surface [8, 57], any involvement of Fe or Si in Zr poisoning can be ruled out.

Based on crystallographic matching, Qiu *et al* [19] proposed a mechanism of Zr poisoning, in which the formation of Al_8Fe_4Zr intermetallic coating on the surface of Al_3Ti particles was responsible for Zr poisoning by decreasing the potency of the Al_3Ti substrate. However, it is well documented in the literature that, in commercial Al-5Ti-1B grain refiner, Al_3Ti is not the nucleant particle responsible for grain refinement of Al-alloys since Al_3Ti dissolves quickly when the grain refiner is added to Al melts with a low concentration of Ti (see reviews in Refs. [4, 5]).

4.3 Mechanism for Zr poisoning

In our previous work [8], we have demonstrated that TiB_2 particles with a clean surface (no elemental segregation) are not potent for heterogeneous nucleation of α-Al and that the formation of the Al_3Ti 2DC on (0 0 0 1) TiB_2 surface is responsible for the enhanced heterogeneous nucleation, leading to significant grain refinement. Enhanced heterogeneous nucleation and thus effective grain refinement can only be achieved by those TiB_2 particles with the Al_3Ti 2DC on their (0 0 0 1) TiB_2 surface. The production process for commercial Al-Ti-B grain refiners is characterized by high concentration of Ti, high temperature and long reaction time [4, 5], which ensures that the TiB_2 particles are fully coated with the Al_3Ti 2DC. From a lattice matching point of view, the formation of such Al_3Ti 2DC on the (0 0 0 1) TiB_2 surface results in a significant reduction of the absolute lattice misfit with α-Al from 4.22% for the TiB_2 without the segregation layer to 0.09% for the TiB_2 with the segregation layer. Consequently, this makes the TiB_2 particles in commercial Al-Ti-B based grain refiners extremely potent for heterogeneous nucleation and thus effective for grain refinement of Al-alloys.

However, the Al_3Ti 2DC on the (0 0 0 1) TiB_2 surface becomes thermodynamically unstable in the presence of Zr in the Al melt, since Al_3Zr has lower free energy of formation than Al_3Ti [58]. In Zr-containing Al-alloy melts, Al_3Ti 2DC dissolves quickly, making the Ti-terminated TiB_2 surface exposed directly to the Zr-containing Al melt. Due to the higher thermodynamic stability of ZrB_2 than that of TiB_2 [9, 55], Zr atoms from the liquid will substitute gradually for some of the Ti atoms in the exposed (0 0 0 1) TiB_2 surface. The substitution process of Zr for Ti atoms on the terminating surface of TiB_2 continues until an ordered Ti_2Zr 2DC structure is established, provided that there are sufficient Zr atoms in the melt and sufficient time for the segregation to take place. Therefore, the Ti_2Zr 2DC forms the new terminating surface of the TiB_2 particle.

The consequence of the formation of the Ti_2Zr 2DC on the (0 0 0 1) TiB_2 surface is that the original potent TiB_2 particles in the commercial Al-Ti-B grain refiners lose their potency for heterogeneous nucleation of α-Al. Since the Ti_2Zr 2DC is completely coherent with (0 0 0 1) TiB_2, the lattice misfit between the Ti_2Zr 2DC and Al will be the same as that between TiB_2 and Al. This means that due to the dissolution of Al_3Ti 2DC and the formation of the Ti_2Zr 2DC as the new terminating surface, the original small lattice misfit 0.09% between Al_3Ti 2DC and (1 1 1) Al is reversed back to the large value 4.22%. This makes the TiB_2 particles with Ti_2Zr 2DC impotent for heterogeneous nucleation of α-Al.

More importantly, the *ab initio* MD simulations in this work show that, at the nucleation temperature, the Zr atoms in the Ti_2Zr 2DC protrude about 0.45 Å from the Ti atom plane towards the liquid Al, resulting in an atomically rough surface (Fig. 8). This atomic roughness on the TiB_2 substrate surface decreases atomic ordering in the liquid adjacent to the liquid/substrate interface and hence impedes heterogeneous nucleation [59], as discussed below.

Prenucleation phenomenon caused by a crystal substrate in an alloy melt at a temperature above the nucleation temperature has been investigated recently by molecular dynamics simulations [50, 59, 60]. It was found that there exists significant atomic ordering in the liquid adjacent to the liquid/substrate interface, which can be taken as a precursor for the subsequent heterogeneous nucleation [50]. Such atomic ordering can be either enhanced by decreasing the lattice misfit between the substrate and the solid [50] and/or increasing the attractive chemical interaction (measured by the heat of mixing) between the substrate and the liquid [60], or impeded by an atomically rough surface of the substrate [59]. Based on the understandings, Zr poisoning can be attributed to the impeding of pre-nucleation on the TiB_2 particles. The formation of the Ti_2Zr 2DC on the (0 0 0 1) TiB_2 surface to replace the original Al_3Ti 2DC results in not only an increase in lattice misfit from 0.09% to 4.22%, but also the roughening of the (0 0 0 1) TiB_2 surface, both of which impede prenucleation and lead to poisoning of the originally potent TiB_2 particles for heterogeneous nucleation.

Therefore, the mechanism for Zr poisoning can be summed up as dissolution of the Al_3Ti 2DC on the (0 0 0 1) TiB_2 surface in the commercial TiB_2 based grain refiners and the formation of the Ti_2Zr 2DC in the Al-Zr melt, which renders TiB_2 particles impotent for heterogeneous nucleation of α-Al. This mechanism for Zr poisoning is consistent with the our experimental observations in this work: (i) the absence of the well-defined OR between TiB_2 and α-Al: (0 0 0 1) [1 1 -2 0] TiB_2 // (1 1 1) [0 -1 1] Al, when Zr is present in Al melt; (ii) only a ppm level of Zr is required even if the Ti_2Zr 2DC is formed on the entire TiB_2 surface; and (iii) Zr poisoning is time dependent [9, 31] and the partial formation of Ti_2Zr 2DC on (0 0 0 1) TiB_2 surface (Fig. 5) due to its slow kinetics of formation in a dilute Al-Zr liquid solution.

The mechanism is consistent with the experimental observations present in this work (Figs. 2 and 5) and in the previous studies in the literature [e.g., 9, 29-31.]. Thermodynamically, a ppm level of Zr addition is sufficient for the formation of the Ti_2Zr 2D layer on the basal surface of all the added TiB_2 particles. Kinetically, the dissolution of the pre-existing Al_3Ti 2DC layer and the formation of the Ti_2Zr 2DC layer will take time to complete, depending upon the temperature and Zr concentration of the melt. It is not expected that all the TiB_2 particles are completely poisoned in a limited period of time. It has been shown in the previous study that the Zr poisoning effect is still increasing with the melt being held at 800°C for over 6 hours [31]. Indeed, our experimental observation shown in Fig. 5 provides the evidence that not all the surface of TiB_2 particles have been covered by Ti_2Zr 2DC layer. It is understandable that a higher concentration of Zr promotes the poisoning, as shown in Fig. 2.

When the addition level of Zr is more than the peritectic composition (0.11%), Al_3Zr particles can possibly act as heterogeneous nucleation sites for α-Al, and may potentially result in grain refinement [29, 30]. In this work, apart from oxides, poisoned TiB_2 and Al_3Zr particles co-exist in the melt with higher Zr contents (>0.11%). In such cases there is an inevitable competition for nucleation between those particles. The lattice misfit with α-Al is 1.34% for Al_3Zr, 3.4% for γ-Al_2O_3 and -4.2% for TiB_2. Although Al_3Zr has the highest potency among these particles, it would not lead to grain refinement due to the large particle size (5 ~ 115 μm in diameter [30]) and thus low particle number density. In cases of Zr poisoning, γ-Al_2O_3 particles are more likely to be responsible for the grain size observed.

4.4 Nucleation control by elemental segregation at the liquid/substrate interface

The epitaxial nucleation model [61] suggests that heterogeneous nucleation precedes layer-by-layer through a structural templating mechanism. It predicts that the nucleation undercooling increases with increasing lattice misfit between the solid and the substrate. This means that heterogeneous nucleation can be controlled by manipulation of the liquid/substrate interface through chemical segregation of the alloying or impurity elements at the interface to either enhance or impede the structural templating. In our previous work, we have demonstrated that segregation of Ti atoms at the interface between the liquid and TiB_2 substrate leads to the formation of Al_3Ti 2DC on the (0 0 0 1) TiB_2 surface, resulting in a substantial reduction of lattice misfit from 4.22% to 0.09%. This makes the TiB_2 particles in the commercial Al-Ti-B grain refiners extremely potent for heterogeneous nucleation of α-Al. In this work, we have demonstrated that segregation of Zr at the liquid/TiB_2 interface leads to the dissolution of the Al_3Ti 2DC on the (0 0 0 1) TiB_2 surface and the formation of the Ti_2Zr 2DC as the new terminating surface of TiB_2, which in turn leads to a significant increase in lattice misfit from the original 0.09% for the TiB_2 particle in the grain refiner to 4.22% for the TiB_2 particle in Al-Zr alloys. Consequently, segregation of Zr atoms onto the TiB_2 surface renders the TiB_2 particles in the Al-Zr melt impotent for heterogeneous nucleation of α-Al, i.e., poisoning the TiB_2 particle by Zr.

In addition, the epitaxial nucleation model [61] predicts that particles with the highest potency will nucleate first since they require the lowest nucleation undercooling. This forms a general rule governing the competition for heterogeneous nucleation between co-existing particles of different potencies in the melt. In Al-alloys, for instance, there are always different types of *in situ* oxide particles in competition for heterogeneous nucleation with the *ex situ* TiB_2 particles from the grain refiner. Most of the oxides in Al-alloys have relatively high potency (small lattice misfit) for heterogeneous nucleation of the α-Al and they are more potent than TiB_2 particles with a clean basal surface (no chemical segregation). Formation of the Al_3Ti 2DC on the (0 0 0 1) TiB_2 surface makes the TiB_2 particles in the Al-Ti-B grain refiner outperform all the *in situ* oxide particles and dominate the nucleation process. However, the formation of the Ti_2Zr 2DC on the TiB_2 surface makes the TiB_2 particles less potent than most of the oxide particles. It is likely that no TiB_2 particles from the Al-Ti-B grain refiner have a chance to participate in the nucleation process in the fully poisoned case.

5. Conclusions

In this work we investigated the mechanism for Zr poisoning through extensive examinations of the Al/TiB_2 interface using advanced electron microscopy and *ab initio* molecular dynamics (MD) simulations. We have confirmed that commercial Al-5Ti-1B grain refiner does not have the ability to refine Al-alloys when a small amount (a few hundred ppm) of Zr is present in the Al melt, resulting in a coarse and fully columnar grain structure after solidification. The well-defined orientation relationship between TiB_2 and Al: (0 0 0 1) [1 1 -2 0] TiB_2 // (1 1 1) [0 -1 1] Al, was not observed after Zr addition, which indicates a reduced nucleation potency of TiB_2 particles in the Zr-containing Al melt.

The state-of-the-art electron microscopy and *ab initio* MD simulations were performed to investigate the mechanism for Zr poisoning. We found that the presence of Zr in Al melts leads to (i) the dissolution of the Al_3Ti 2-diemntional compound (2DC) formed on the (0 0 0 1) TiB_2 surface during the grain refiner production process; and (ii) the formation of an atomic monolayer of Ti_2Zr (Ti_2Zr 2DC) on the (0 0 0 1) TiB_2 surface, which replaces the original Ti-terminated TiB_2 surface. This results in a significant increase in lattice misfit from the original 0.09% (between α-Al and TiB_2 with Al_3Ti 2DC) to 4.22% (between α-Al and TiB_2 with Ti_2Zr 2DC), rendering TiB_2 particles in Al-Zr melts impotent for heterogeneous nucleation of α-Al.

Ab initio MD simulations have confirmed that the Ti_2Zr 2DC formed on the (0 0 0 1) TiB_2 surface is atomically rough. This atomic roughness can be attributed to the facts that Zr atoms have a larger atomic size and a stronger attractive chemical interaction with liquid Al in comparison with Ti atoms in the Ti_2Zr 2DC. According to the recent MD simulation results [59], this atomically rough surface weakens atomic ordering in the liquid adjacent to the liquid/substrate interface and consequently hinders heterogeneous nucleation.

The mechanism for Zr poisoning can, therefore, be summed up as dissolution of the Al_3Ti 2DC on the (0 0 0 1) TiB_2 surface in the commercial Al-Ti-B based grain refiner and the formation of the Ti_2Zr 2DC on TiB_2 basal surface in the Al-Zr melt, which renders TiB_2 particles impotent for heterogeneous nucleation of α-Al due to the increased lattice misfit and surface roughness at atomic level.

In addition, we have found that there is no segregation of Fe or Si at the basal surface of TiB_2, although Fe was found to segregate on the {1 0 -1 0} TiB_2 prismatic surface. This confirms that neither Fe nor Si (as impurity elements) played any role in Zr poisoning of TiB_2 particles in the Zr-containing Al melt.

Furthermore, this work, in combination of our previous work [8], demonstrates that heterogeneous nucleation can be effectively manipulated, either enhanced or impeded, by chemical segregation of selected alloying/ impurity elements at the liquid/substrate interface.

Acknowledgements

Financial support from the EPSRC (UK) under grant number EP/N007638/1 is gratefully acknowledged. Thanks go to Mr Shihao Wang from BCAST, Brunel University London for his help in the simulation of STEM HAADF images.

References

[1] ASM Handbook, vol. 15 Casting. Metals Park, ASM, OH, 2008.
[2] L. Greer, Overview: application of heterogeneous nucleation in grain-refining of metals, J. Chem. Phys. 145 (2016) 211704.1-211704.14.
[3] A. Cibula, The grain refinement of aluminium alloy castings by additions of titanium and boron, J. Inst. Metals 80 (1951-52) 1-16.
[4] D.G. McCartney, Grain refining of aluminium and its alloys using inoculants, Inter. Mater. Rev. 34 (1989) 247-260.
[5] B.S. Murty, S.A. Kori, M. Chakraborty, Grain refinement of aluminium and its alloys by heterogeneous nucleation and alloying, Inter. Mater. Rev. 47 (2002) 3-47.
[6] T.E. Quested, Understanding mechanisms of grain refinement of aluminium alloys by inoculation, Mater. Sci. Tech. 20 (2004) 1357-1369.
[7] M.A. Easton, M. Qian, A. Prasad, D.H. StJohn, Recent advances in grain refinement of light metals and alloys, Current Opinion in Solid State and Mater. Sci. 20 (2016) 13-24.
[8] Z. Fan, Y. Wang, Y. Zhang, T. Qin, X.R. Zhou, G.E. Thompson, T. Pennycook, T. Hashimoto, Grain refining mechanism in the Al/Al-Ti-B system, Acta Mater. 84 (2015) 292-304.
[9] G.P. Jones, J. Pearson, Factors affecting the grain-refinement of aluminum using titanium and boron additives, Metall. Trans. B, 7B (1976) 223-234.
[10] M.E.J. Birch, P. Fisher, Grain refining of commercial aluminium alloys with titanium boron aluminium, in: T. Shepard (Ed.), Proc. of the Conference on Aluminium Technology 86, The Institute of Metals, London, 1986, pp. 117-124.
[11] S.M. Ahmady, D.G. McCartney, S.R. Thistlethwaite, Assessment of aluminium grain refiner performance using the ALCOA test, in: C.M. Bickert (Ed.), Light Metals 1990, Warrendale, PA, TMS 1990, pp. 837-843.

[12] M.A. Kearns, P. Cooper, Effects of solutes on grain refinement of selected wrought aluminium alloys, Mater. Sci. Technol. 13 (1997) 650-654.
[13] M.E.J. Birch, A.J.J. Cowell, Grain refinement of aluminium alloys containing chromium and zirconium, in: J. Beech, H. Jones (Eds.), Solidification Processing 1987, The Institute of Metals, London, 1988, pp. 149-152.
[14] A.A. Abdel-Hamid, Effect of other elements on the grain refinement of Al by Ti or Ti and B. Part I- A critical review, Z. Metallkd. 80 (1989) 566-569.
[15] A.A. Abdel-Hamid, Effect of other elements on the grain refinement of aluminum by titanium or titanium and boron. Part II. Effect of the refractory metals vanadium, molybdenum, zirconium, and tantalum, Z. Metallkd. 80 (1989) 643-647.
[16] M.E.J. Birch, Grain refining of aluminium-lithium based alloys with tiatanium boron aluminium. In: C. Baker, P.J. Gregson, S.J. Harris, C.J. Peers (Eds.), Aluminium-Lithium Alloys III, The Institute of Metals, London, 1986, pp. 152-158.
[17] J.A. Spittle, S. Sadli, The influence of zirconium and chromium on the grain-refining efficiency of Al-Ti-B inoculants, Cast Metals 8 (1995) 247-253.
[18] J.A. Spittle, S. Sadli, Effect of alloy variables on grain refinement of binary aluminium alloys with Al-Ti-B, Mater. Sci. Technol. 11 (1995) 533-537.
[19] D. Qiu, J.A. Taylor, M.-X. Zhang, Understanding the co-poisoning effect of Zr and Ti on the grain refinement of cast aluminium alloys, Metall. Mater. Trans. A, 41A (2010) 3412-3421.
[20] M. Johnsson, Influence of Zr on the grain refinement of aluminium, Z. Metallkd. 85 (1994) 786-789.
[21] A. Arjuna Rao, B.S. Murty, M. Chakraborty, Influence of chromium and impurities on the grain-refining behavior of aluminum, Metall. Mater. Trans. A, 27A (1996) 791-800.
[22] A. Arjuna Rao, B.S. Murty, M. Chakraborty, Response of an Al-Cr alloy towards grain refinement by Al-5Ti-lB master alloy, Int. J. Cast Met. Res. 9 (1996) 125-132.
[23] C.R. Chakravorty, M. Chakraborty, Grain refining of Al-Li alloy with Al-Ti-B, Cast Metals, 4 (1991) 98-100.
[24] G.K. Sigworth and M.M. Guzowaski, Grain refining of hypoeutectic Al-Si alloys, AFS Trans. 93 (1985) 907-912.
[25] A. Arjuna Rao, B.S. Murty, M. Chakraborty, Role of zirconium and impurities in grain refinement of aluminium with Al-Ti-B, Mater. Sci. Tech. 13 (1997) 769-777.
[26] D. Qiu, J.A. Taylor, M.-X. Zhang, P.M. Kelly, A mechanism for the poisoning effect of silicon on the grain refinement of Al-Si alloys, Acta Mater. 55 (2007) 1447-1456.
[27] M. Easton, D. StJohn, Grain Refinement of Aluminium Alloys: Part I. The nucleant and solute paradigms—A review of the literature, Metall. Mater. Trans. A, 30A (1999) 1613-1623.
[28] M. Easton, D. StJohn, An analysis of the relationship between grain size, solute content, and the potency and number density of nucleant particles, Metall. Maters. Trans. A, 36A (2005) 1911-1920.
[29] J.A. Marcantonio, L.F. Mondolfo, Nucleation of aluminium by several intermetallic compounds, J. Inst. Met., 98 (1970) 23-27.
[30] F. Wang, D. Qiu, Z.-L. Liu, J.A. Taylor, M.A. Easton, M.-X. Zhang, The grain refinement mechanism of cast aluminium by zirconium, Acta Mater. 61 (2013) 5636-5645.
[31] A.M. Bunn, P. Schumacher, M.A. Kearns, C.B. Boothroyd, A.L. Greer, Grain refinement by Al-Ti-B alloys in aluminium melts: a study of the mechanisms of poisoning by zirconium, Mater. Sci. Technol. 15 (1999) 1115-1123.
[32] G.P. Jones, Grain refinement of castings using inoculants for nucleation above liquidus, in: J. Beech, H. Jones (Eds.), Solidification Processing 1987, The Institute of Metals, London, 1988, pp. 496-499.
[33] P. Schumacher, P. Cizek, A. Bunn, Zr-poisoning of grain refiner particles studied in Al-Ni-Zr amorphous alloys, in: J.F. Grandfield, D.G. Eskin (Eds.), Essential Readings in Light Alloys: Cast Shop for Aluminium Alloy Production, Warrendale, PA, TMS, 2013, pp. 381-386.
[34] A.J. Whitehead, S.A. Danilak, D.A. Granger, The Development of a commercial Al-3%Ti-

0.15%C grain refining master alloy, in: R. Huglen (Ed.), Light Metals 1997, Warrendale, PA, TMS, 1997, pp. 785-793.
[35] W. Schneider, M.A. Kearns, M.J. McGarrry, A.J. Whitehead, A comparison of the behaviour of AlTiB and AlTiC grain refiner, in: J.F. Grandfield, D.G. Eskin (Eds.), Essential Readings in Light Alloys: Cast Shop for Aluminium Alloy Production, Warrendale, PA, TMS, 2013, pp. 400-408.
[36] Y. Birol, Grain refining efficiency of Al-Ti-C alloy, J. Alloys Compd. 422 (2006) 128-131.
[37] G.S. Vinod Kumar, B.S. Murty, M. Chakraborty, Development of Al-Ti-C grain refiners and study of their grain refining efficiency on Al and Al-7Si alloy, J. Alloys Compd. 396 (2005) 143-150.
[38] H.M. Ding, X.F. Liu, L.N. Yu, Influence of zirconium on grain refining efficiency of Al-Ti-C master alloys, J. Mater. Sci. 42 (2007) 9817-9821.
[39] Standard test procedure for aluminium alloy grain refiners (TP-1). Washington, DC: The Aluminium Association; 1990.
[40] Z. Fan, Y. Wang, M. Xia, S. Arumuganathar, Enhanced heterogeneous nucleation in AZ91D alloy by intensive melt shearing, Acta Mater. 57 (2009) 4891-4901.
[41] Y. Wang, Z. Fan, X. Zhou, G.E. Thompson, Characterisation of magnesium oxide and its interface with α-Mg in Mg-Al based alloys, Philo. Mag. Lett. 91 (2011) 516-529.
[42] C. Koch, Determination of core structure periodicity and point defect density along dislocations, Ph.D. Thesis, Arizona State University, 2002.
[43] G. Kresse, J. Hafner, *Ab initio* molecular-dynamics simulation of the liquid-metal–amorphous-semiconductor transition in germanium, Phys. Rev. B, 49 (1994) 14251-14269.
[44] G. Kresse, J. Furthmüller, Efficiency of *ab-initio* total energy calculations for metals and semiconductors using a plane-wave basis set, Comp. Mater. Sci. (1996) 15-50.
[45] P.E. Blöchl, Projector augmented-wave method, Phys. Rev. B, 50 (1994) 17953-17979.
[46] G. Kresse, J. Joubert, From ultrasoft pseudopotentials to the projector augmented-wave method, Phys. Rev. B, 59 (1999) 1758-1775.
[47] J.P. Perdew, K. Burke, M. Ernzerhof, Generalized gradient approximation made simple, Phys. Rev. Lett. 77 (1996) 3865-3868.
[48] H. J. Monkhorst, J. D. Pack, Special points for Brillouin-zone integrations, Phys. Rev. B, 13 (1976) 5188-5192.
[49] A.L. Greer, A.M. Bunn, A. Tronche, P.V. Evans, D.J. Bristow, Modelling of inoculation of metallic melts: application to grain refinement of aluminium by Al-Ti-B, Acta Mater. 48 (2000) 2823-2835.
[50] H. Men, Z. Fan, Prenucleation induced by crystalline substrates, Metall. Mater. Trans. A, 49A (2018) 2766-2777.
[51] S. K. Dolukhanyan A. G. Aleksanyan, O.P. Ter-Galstyan, V.Sh. Shekhtman, M.K. Sakharov, G.E. Abrosimova, Specifics of the formation of alloys and their hydrides in Ti–Zr–H system, Russian J. of Phys. Chem. B, 1 (2007) 563-569.
[52] I.P. Swainson, S.K. Dolukanyan, A.G. Aleksanyan, V.Sh. Shekhtman, D.G. Mayilyan, A.L. Yonkeu, Omega-phase in Ti-Hf-Zr alloys produced by the hydride-cycle method, Can. J. Phys. 88 (2010) 741-749.
[53] S. K. Dolukhanyan, A. G. Aleksanyan, O.P. Ter-Galstyan, D.G. mayilyan, V.Sh. Shekhtman, M.K. Sakharov, S.S. Khasanov, The Peculiarities of formation of alloys structure in the system Ti-Zr-Hf-H, in: B. Baranowski, S.Y. Zaginaichenko, D.V. Schur, V.V. Skorokhod and A. Veziroglu (Eds.), Carbon Nanomaterials in Clean Energy Hydrogen Systems, Springer, 2008, pp. 733-741.
[54] P. Zhang, F. Meng, Z. Gong, G. Ji, S. Cui, D.Q. Wei, First-principles study of structure and properties of ω-Ti_2Zr, Comp. Mater. Sci. 74 (2013) 129-137.
[55] A. Khaliq, M.A. Rhamdhani, G.A. Brooks, J. Grandfield, Thermodynamic analysis of Ti, Zr, V and Cr impurities in aluminium melt, in: S.J. Lindsay (Ed.), Light Metals 2011, Warrendale, PA, TMS, 2011, pp. 751-756.

[56] P.A. Farrar, S. Adler, On the system titanium-zirconium, Trans. Metall. Soc. AIME, 236 (1966) 1061-1064.
[57] P Schumacher, A.L. Greer, Enhanced heterogeneous nucleation of α-Al in amorphous aluminium alloys, Mater. Sci. Eng. A, A181/A182 (1994) 1335-1339.
[58] G. Ghosh, S. Vaynman, M. Asta, M.E. Fine, Stability and elastic properties of L12-$(Al,Cu)_3(Ti,Zr)$ phases: *Ab initio* calculations and experiments, Intermetallics 15 (2007) 44-54.
[59] B. Jiang, H. Men, Z. Fan, Atomic ordering in the liquid adjacent to an atomically rough solid surface, Comp. Mater. Sci. 153 (2018) 73-81.
[60] C.M. Fang, H. Men, Z. Fan, Effect of substrate chemistry on prenucleation, Metall and Mat Trans A (2018). https://doi.org/10.1007/s11661-018-4882-y.
[61] Z. Fan, An epitaxial model for heterogeneous nucleation on potent substrates, Metall. Mater. Trans. A, 44A (2013) 1409-1418.

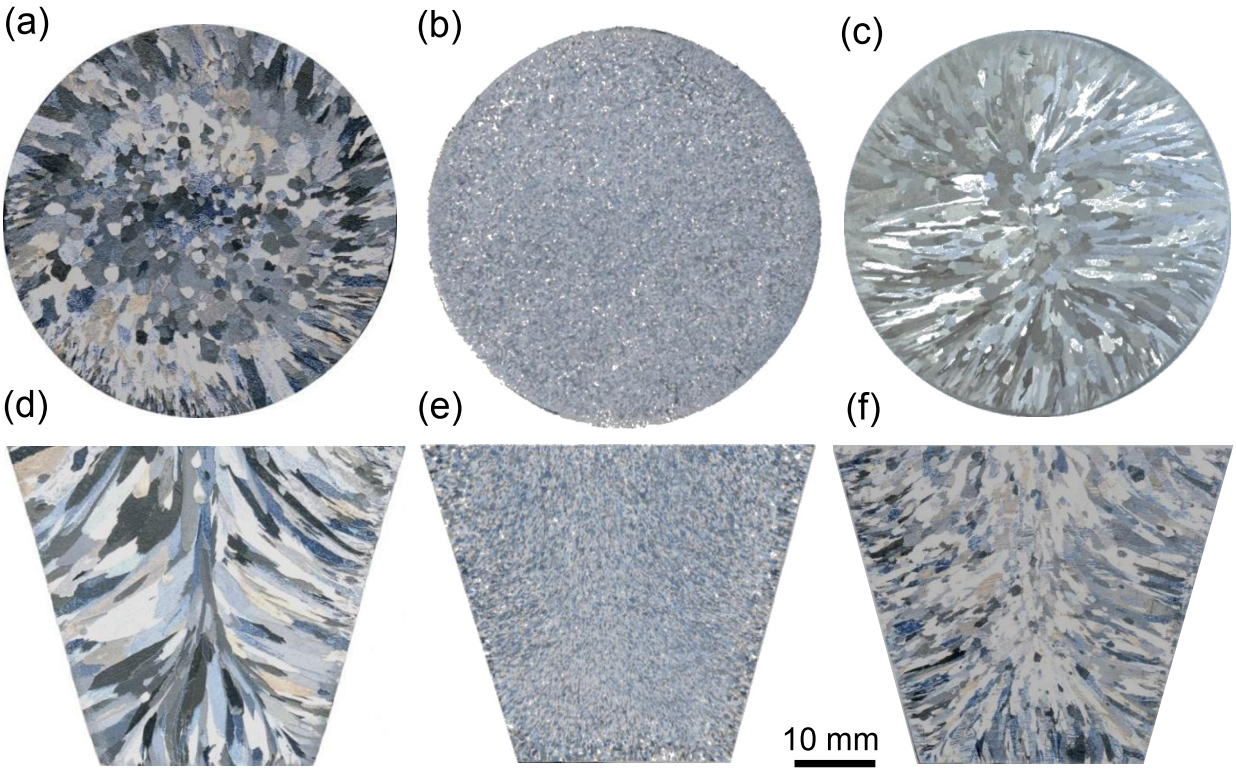

Fig. 1 Macrographs showing grain structure on (a-c) transverse and (d-f) longitudinal sections of CP-Al samples solidified in the TP-1 mould, with (a, d) no addition, (b, e) addition of 0.1% commercial Al-5Ti-1B grain refiner, and (c, f) additions of both 0.1% of the grain refiner and 0.058% (558 ppm) Zr, showing that the grain refiner has no ability to refine the CP-Al when the small amount of Zr is present.

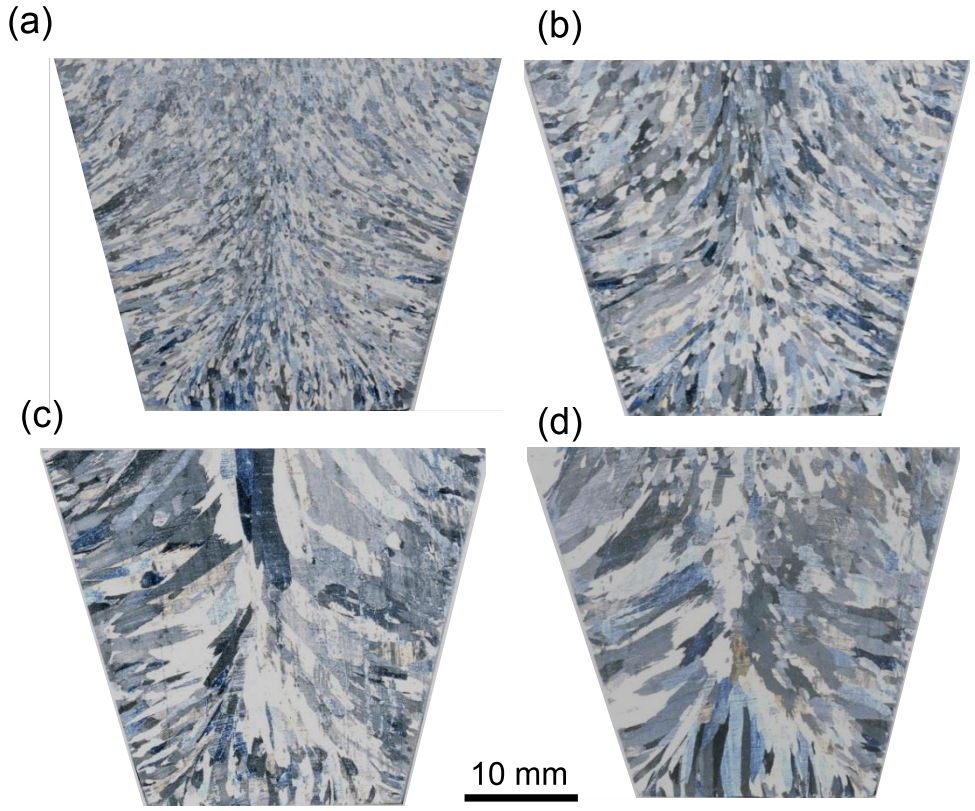

Fig. 2 Macrographs showing the grain structure on longitudinal sections of Al-Zr alloy samples solidified in the TP-1 mould, containing 0.1% commercial Al-5Ti-1B grain refiner and with increasing additions of Zr: (a) 0.088%, (b) 0.206%, (c) 0.310%, and (d) 0.450%. The grain structure remains columnar and the width of the columnar grains increases with increasing Zr concentration.

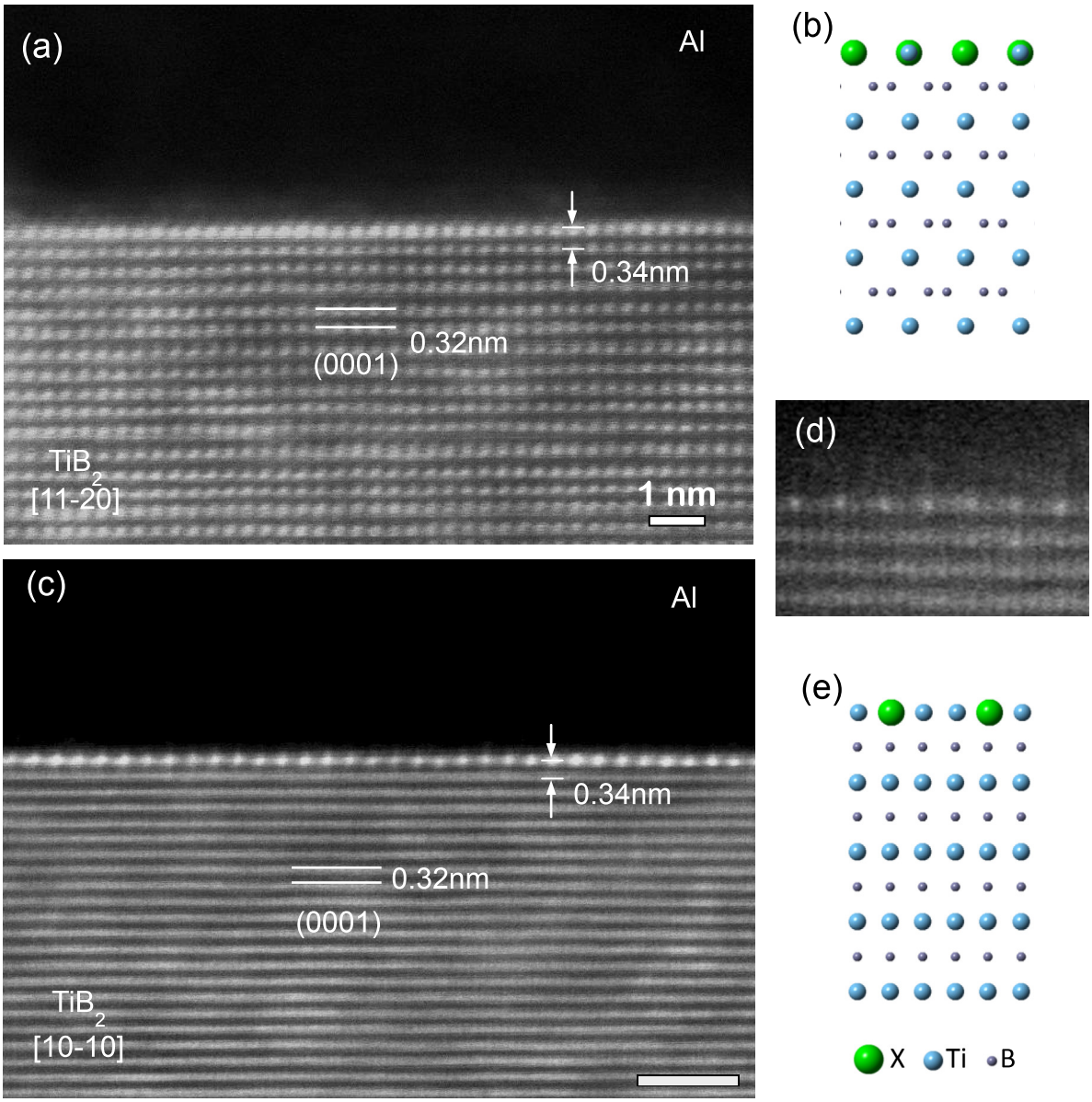

Fig. 3 (a, c) High resolution STEM Z-contrast HAADF images showing an atomic mono-layer containing heavier atoms X (brighter contrast than Ti) on the (0 0 0 1) surface of TiB_2 particle being viewed along (a) [1 1 -2 0] and (c) [1 0 -1 0] directions respectively, (d) SuperSTEM HAADF image at higher resolution showing the periodic variation in brightness of the atomic columns of the segregation monolayer. The corresponding schematics in (b, e) show the possible atomic arrangement across the Al/TiB_2 interface along the two directions (the large green spheres represent the heavier atoms X).

Fig 4

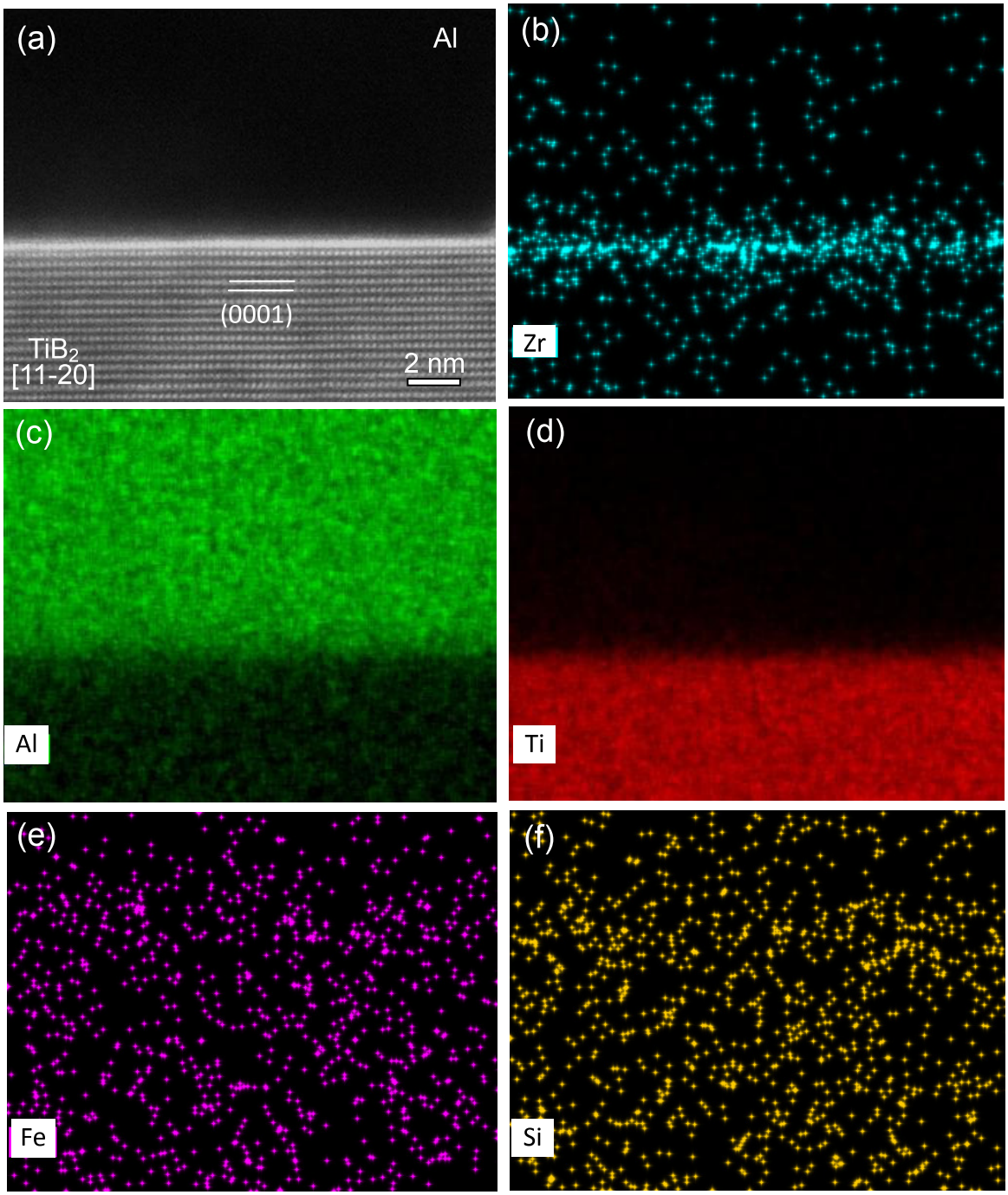

Fig. 4 (a) High resolution STEM HAADF image across Al/TiB_2 interface viewed along [1 1 -2 0]TiB_2 direction, and (b-f) Super-X EDS elemental mapping of (b) Zr (cyan), (c) Al (green), (d) Ti (red), (e) Fe (purple) and (f) Si (yellow) across the interface, showing Zr segregation but no segregation of Fe and Si at the interface between Al and (0 0 0 1) basal plane surface of TiB_2.

Fig 5

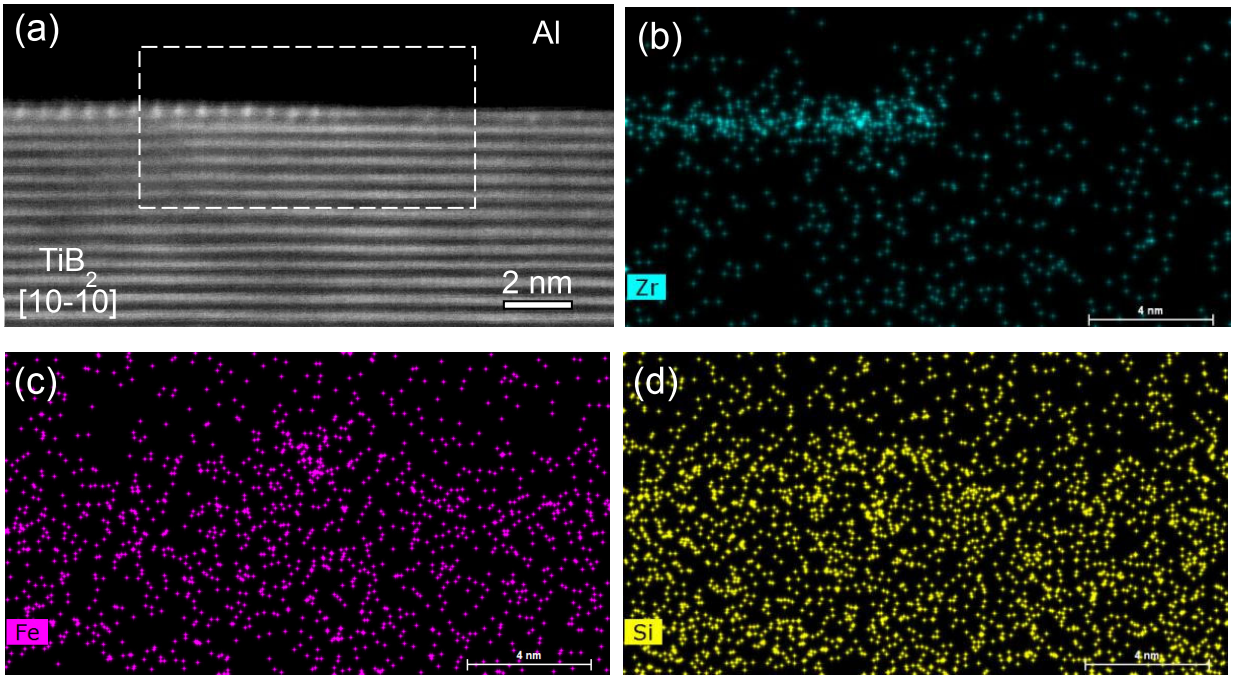

Fig. 5 (a) High resolution STEM HAADF image across Al/TiB_2 interface viewed along [1 0 -1 0] TiB_2 direction, and (b-d) Super-X EDS elemental mapping (from the marked area in (a)) of (b) Zr (cyan), (c) Fe (purple) and (d) Si (yellow) across the interface, showing the on-going Zr segregation process on the (0 0 0 1) surface of a TiB_2 particle evidenced by the periodic pattern of brightness in (a) the HAADF images and the Zr composition profile in (b) the EDS map on the left hand part of the TiB_2 surface. No segregation of Fe and Si is observed at the interface.

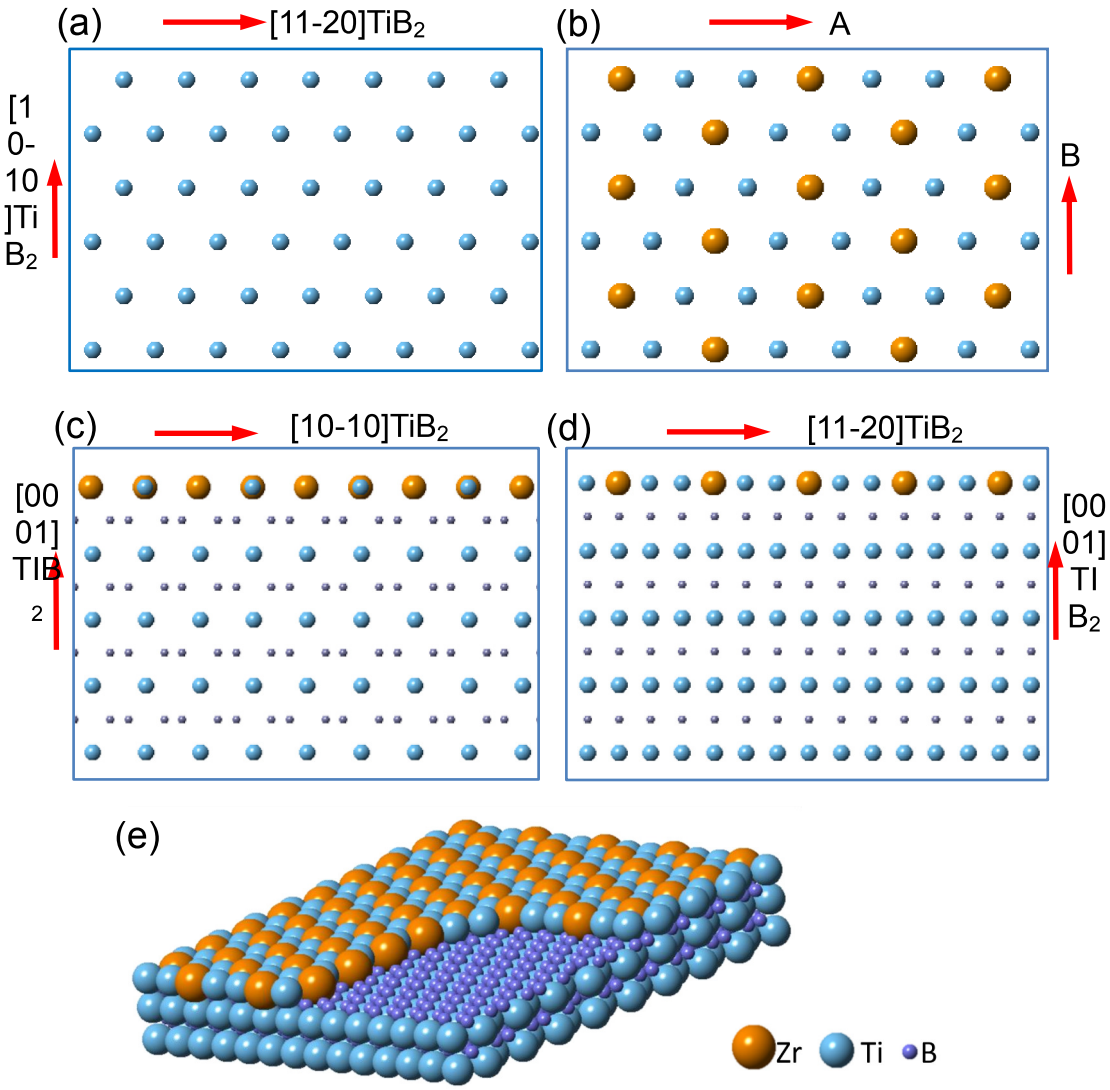

Fig. 6 Schematic illustrations showing (a, b) arrangement of (a) Ti atoms in (0 0 0 1)Ti planes of TiB_2 and (b) Ti and Zr atoms in the Ti_2Zr 2DC; (c, d) side view of TiB_2 (Ti_2Zr 2DC) along (c) [1 1 -2 0]TiB_2 and (d) [1 0 -1 0]TiB_2 direction, respectively; and (e) 3D construction of the Ti_2Zr 2DC on top of TiB_2.

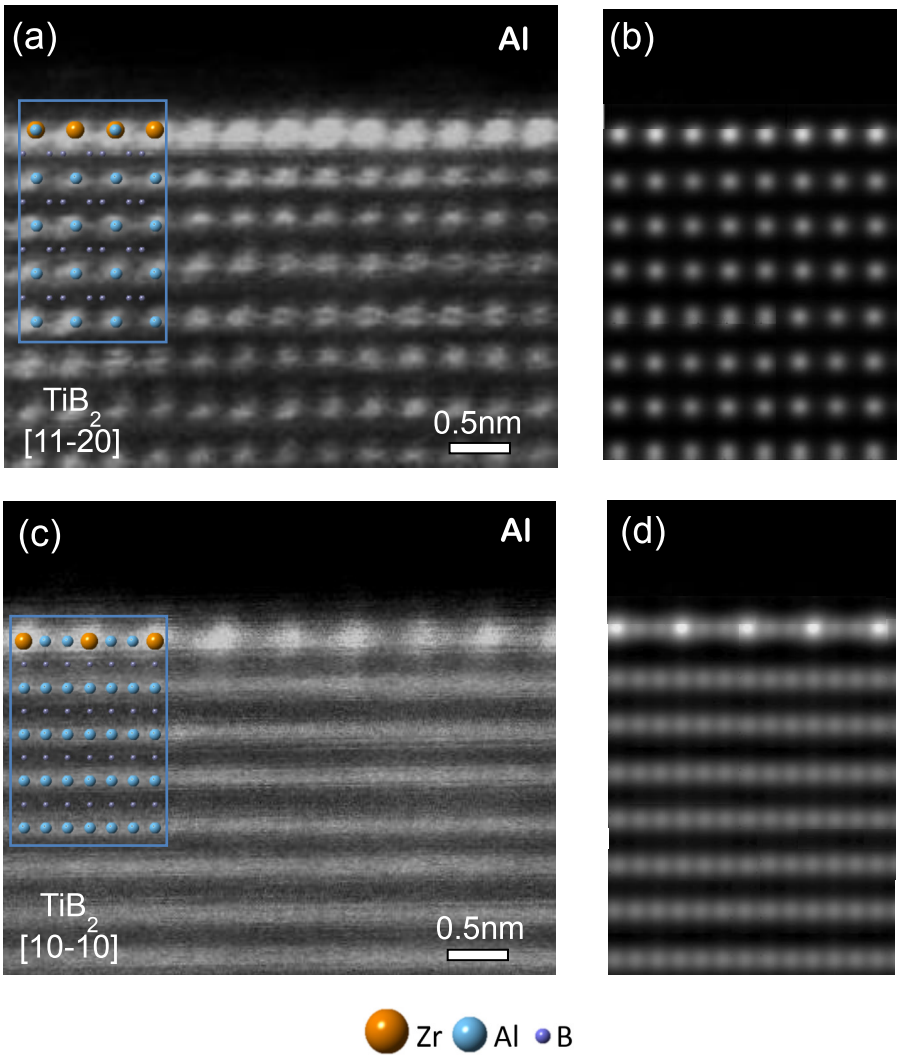

Fig. 7 (a, c) Experimental STEM HAADF images compared with (b, d) the simulated HAADF images along (a, b) [1 1 -2 0] and (c, d) [1 0 -1 0] TiB_2 direction, respectively. The simulation of STEM HAADF images was carried out using the QSTEM multislice simulation package developed by Koch [41], according to the constructed super-lattice structure of Ti_2Zr 2DC on the (0 0 0 1) surface of TiB_2 as shown schematically in Figs. 6b, 6c and 6d.

Figs 8, 9, 10

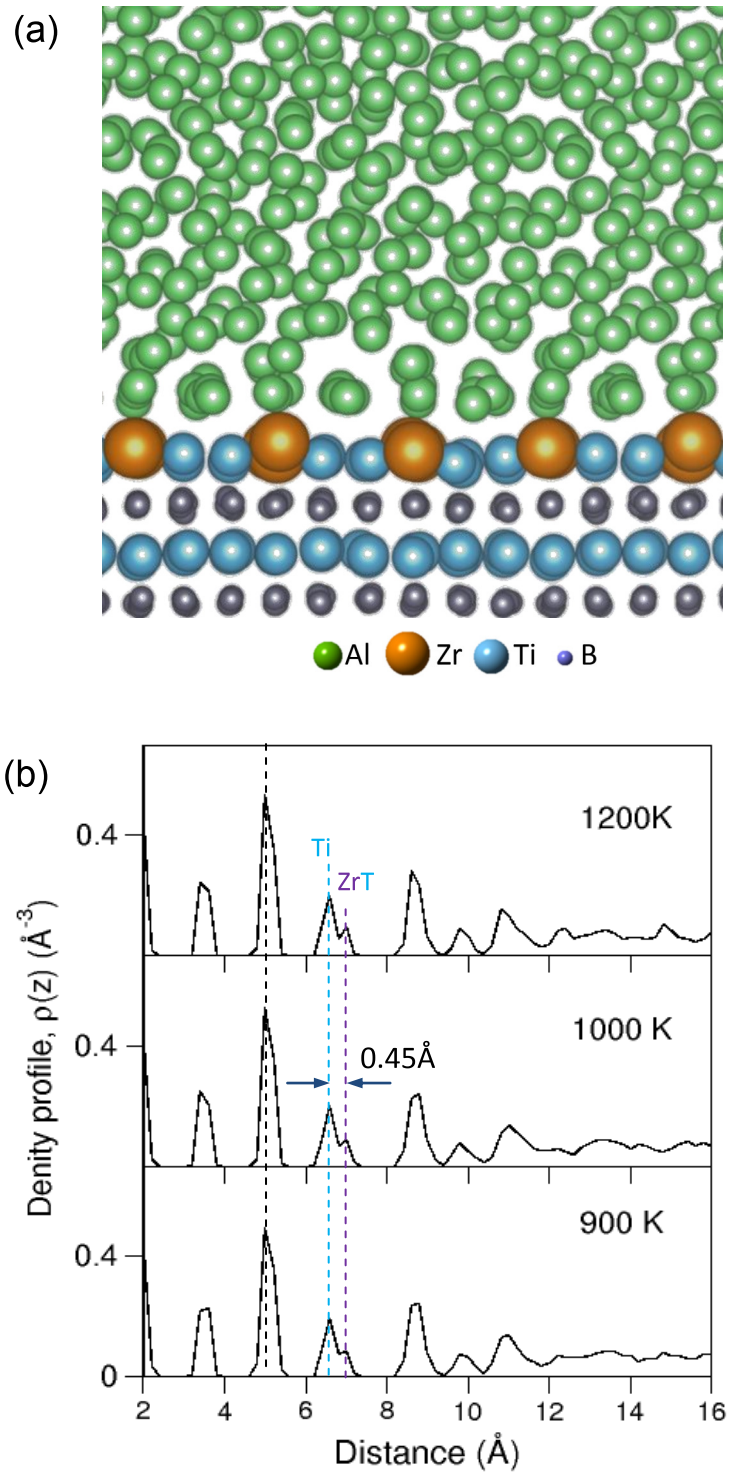

Fig. 8 (a) Snapshot of Al(liquid)/TiB_2(Ti_2Zr 2DC) interface along [1 0 -1 0] TiB_2(Ti_2Zr 2DC) direction simulated at 1000 K, and (b) atomic density profiles ρ(z) across the Al(liquid)/TiB_2 (Ti_2Zr 2DC) interface simulated at 900 K, 1000 K and 1200 K, respectively. The dotted lines in (b) indicate the position of the Ti and Zr atoms in the Ti_2Zr 2DC.

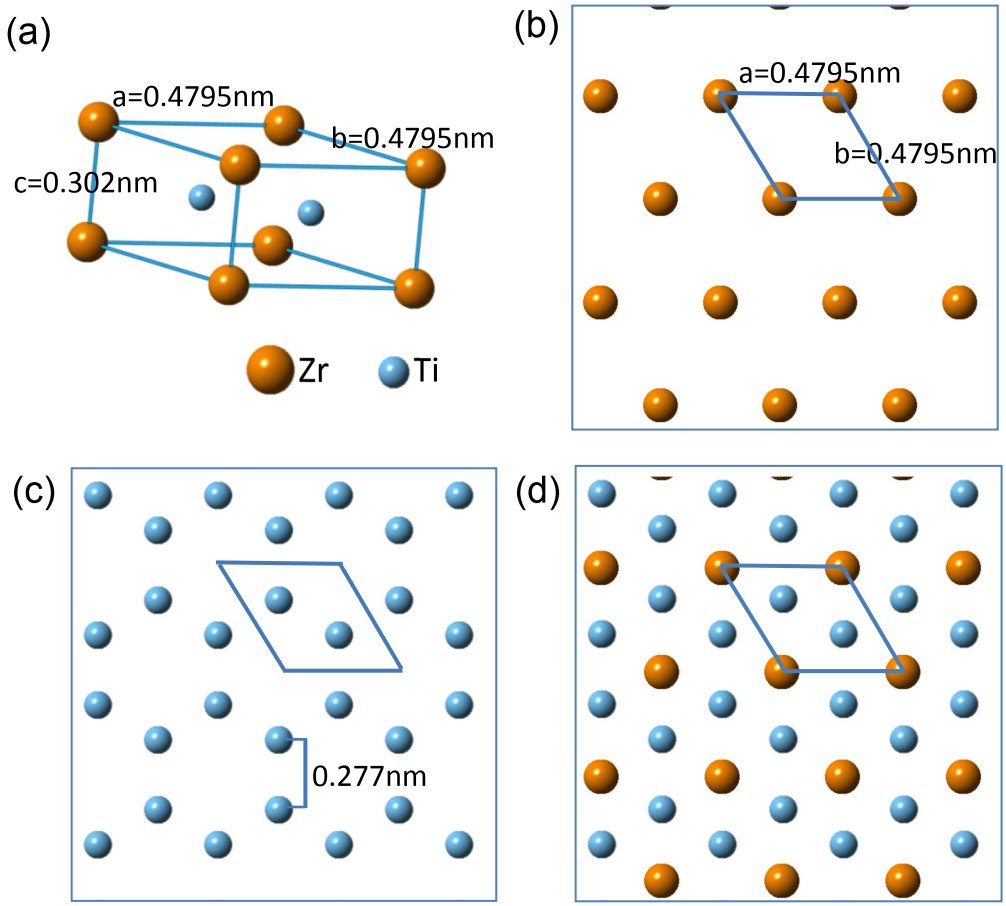

Fig. 9 Schematics showing (a) the unit cell of ω-Ti_2Zr phase [50] stacked by alternating Zr and Ti planes, (b, c) arrangement of Zr atoms in (0 0 0 1) Zr plane and Ti atoms in (0 0 0 1) Ti plane of ω-Ti_2Zr phase respectively, and (d) atomic configuration of a Ti_2Zr 2DC structure constructed by superimposition of the Zr and Ti planes of ω-Ti_2Zr phase.

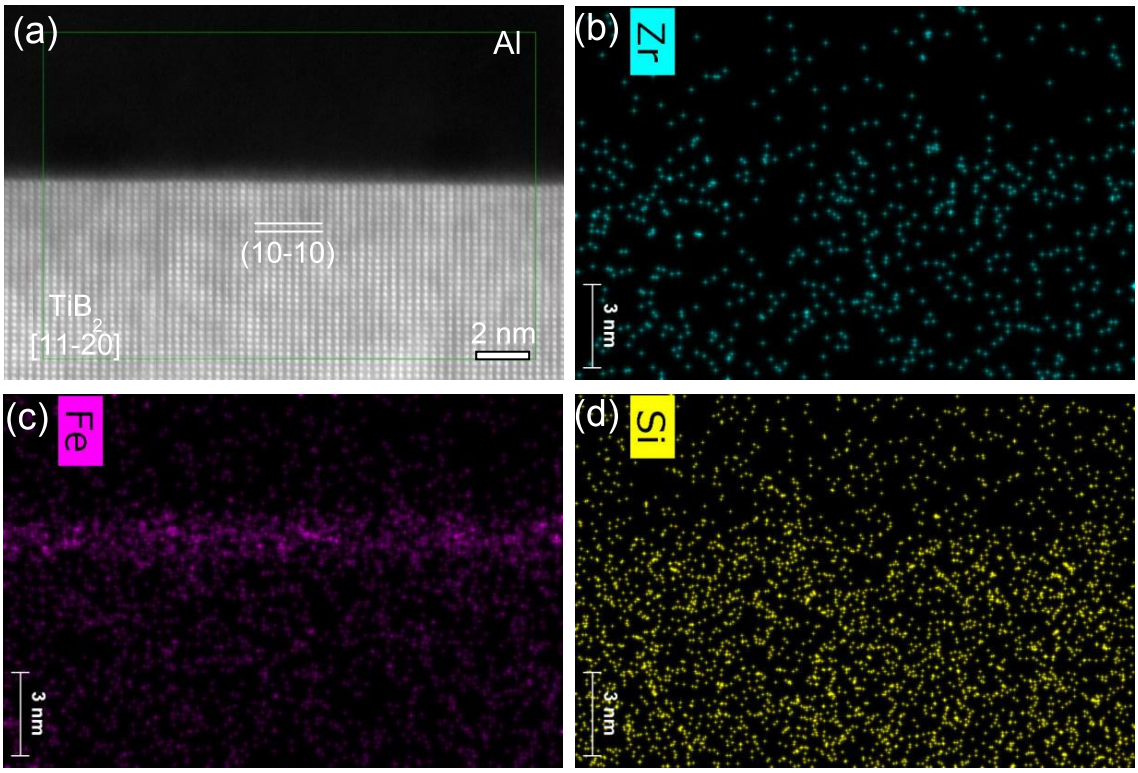

Fig. 10 (a) STEM HAADF image of Al/ (1 0 -1 0)TiB_2 interface and (b-d) STEM SuperX-EDS elemental mapping (from the marked area) of (b) Zr, (c) Fe and (d) Si across the interface, showing Fe segregation but no Zr or Si segregation at the interface between Al and the prismatic surface of TiB_2.

Table 1

Table 1 Compositions (wt.%) of commercial purity Al (CP-Al), Al-5Ti-1B grain refiner and Al-10Zr master alloy used in this work.

Alloy	Fe	Si	V	Zn	Ni	Cu	Cr	Ti	B	Zr	Al
CP-Al	0.08	0.03	-	0.003	0.005	0.001	0.001	0.006	-	-	Bal.
Al-5Ti-1B	0.09	0.08	0.04	-	-	-	-	4.80	0.85	-	Bal.
Al-10Zr	0.08	0.03	-	0.01	-	0.04	0.02	-	-	9.90	Bal.